RAPID COMMUNICATION

Electronic structure, Dirac points and Fermi arc surface states in three-dimensional Dirac semimetal Na_3Bi from angle-resolved photoemission spectroscopy*

Aiji Liang(梁爱基)[1], Chaoyu Chen(陈朝宇)[1], Zhijun Wang(王志俊)[1], Youguo Shi(石友国)[1], Ya Feng(冯娅)[1], Hemian Yi(伊合绵)[1], Zhuojin Xie(谢卓晋)[1], Shaolong He(何少龙)[1,†], Junfeng He(何俊峰)[1], Yingying Peng(彭莹莹)[1], Yan Liu(刘艳)[1], Defa Liu(刘德发)[1], Cheng Hu(胡成)[1], Lin Zhao(赵林)[1], Guodong Liu(刘国东)[1], Xiaoli Dong(董晓莉)[1], Jun Zhang(张君)[1], M Nakatake[2], H Iwasawa[2], K Shimada[2], M Arita[2], H Namatame[2], M Taniguchi[2], Zuyan Xu(许祖彦)[3], Chuangtian Chen(陈创天)[3], Hongming Weng(翁红明)[1,4], Xi Dai(戴希)[1,4], Zhong Fang(方忠)[1,4], and Xing-Jiang Zhou(周兴江)[1,4,‡]

[1] *Beijing National Laboratory for Condensed Matter Physics, Institute of Physics, Chinese Academy of Sciences, Beijing* 100190, *China*
[2] *Hiroshima Synchrotron Radiation Center, Hiroshima University,* 2-313 *Kagamiyama, Higashi-Hiroshima City,* 739-0046, *Japan*
[3] *Technical Institute of Physics and Chemistry, Chinese Academy of Sciences, Beijing* 100190, *China*
[4] *Collaborative Innovation Center of Quantum Matter, Beijing, China*

(Received 12 May 2016; revised manuscript received 3 June 2016; published online 10 June 2016)

The three-dimensional (3D) Dirac semimetals have linearly dispersive 3D Dirac nodes where the conduction band and valence band are connected. They have isolated 3D Dirac nodes in the whole Brillouin zone and can be viewed as a 3D counterpart of graphene. Recent theoretical calculations and experimental results indicate that the 3D Dirac semimetal state can be realized in a simple stoichiometric compound A_3Bi (A = Na, K, Rb). Here we report comprehensive high-resolution angle-resolved photoemission (ARPES) measurements on the two cleaved surfaces, (001) and (100), of Na_3Bi. On the (001) surface, by comparison with theoretical calculations, we provide a proper assignment of the observed bands, and in particular, pinpoint the band that is responsible for the formation of the three-dimensional Dirac cones. We observe clear evidence of 3D Dirac cones in the three-dimensional momentum space by directly measuring on the k_x–k_y plane and by varying the photon energy to get access to different out-of-plane k_zs. In addition, we reveal new features around the Brillouin zone corners that may be related with surface reconstruction. On the (100) surface, our ARPES measurements over a large momentum space raise an issue on the selection of the basic Brillouin zone in the (100) plane. We directly observe two isolated 3D Dirac nodes on the (100) surface. We observe the signature of the Fermi-arc surface states connecting the two 3D Dirac nodes that extend to a binding energy of ∼150 meV before merging into the bulk band. Our observations constitute strong evidence on the existence of the Dirac semimetal state in Na_3Bi that are consistent with previous theoretical and experimental work. In addition, our results provide new information to clarify on the nature of the band that forms the 3D Dirac cones, on the possible formation of surface reconstruction of the (001) surface, and on the issue of basic Brillouin zone selection for the (100) surface.

Keywords: Dirac semimetal, Na_3Bi, photonemission, surface state

PACS: 71.20.–b, 73.20.–r, 79.60.Bm, 03.65.Pm **DOI:** 10.1088/1674-1056/25/7/077101

1. Introduction

The Dirac semimetals have isolated bulk Fermi nodes in the momentum space of the whole Brillouin zone, which are generated by a linear touching of the conduction band and the valence band.[1–32] In the vicinity of these Fermi nodes, the associated bands disperse linearly along all the three momentum directions and can be effectively described by massless Dirac equation. Thus, the isolated Fermi nodes are 3D Dirac nodes and Dirac semimetals can ideally mimic graphene[33,34] in three dimensions. Dirac semimetals are new topological states that are different from topological insulators[35,36] but closely related to Weyl semimetals.[1,9–14,37–45] The low-energy excitations of a Weyl semimetal is analogous to a Weyl fermion which can be described by Weyl equation,[37] which is a half of the massless Dirac equation. Therefore, a Dirac node in a 3D Dirac semimetal can be viewed as a pair of Weyl nodes with opposite chirality, which usually tend to annihilate each other when they overlap in momentum space. In crystal systems, however, such a Dirac node can survive under the protection of a certain crystallographic symmetry.[15] Recently, A_3Bi (A = Na, K, Rb) are predicted to be Dirac semimetals, which

*Project supported by the National Natural Science Foundation of China (Grant No. 11574367), the National Basic Research Program of China (Grant Nos. 2013CB921700, 2013CB921904, and 2015CB921300), and the Strategic Priority Research Program (B) of the Chinese Academy of Sciences (Grant No. XDB07020300). The synchrotron radiation experiments have been done under the HiSOR Proposal numbers, 12-B-47 and 13-B-16.

†Corresponding author. E-mail: XJZhou@aphy.iphy.ac.cn
‡Corresponding author. E-mail: shaolonghe@aphy.iphy.ac.cn

© 2016 Chinese Physical Society and IOP Publishing Ltd

have a pair of isolated 3D bulk Dirac nodes along the A–Γ–A direction at the Fermi level.[16] The robustness of the Dirac nodes are guaranteed by the crystal symmetry of A_3Bi (A = Na, K, Rb). Moreover, topological non-trivial surface states are expected on the specific (100) crystalline surface of A_3Bi (A = Na, K, Rb), showing up as fascinating Fermi arcs nesting the two bulk Dirac nodes at the Fermi level. A_3Bi (A = Na, K, Rb) can be driven into various topologically distinct state such as Weyl semimetals, topological insulators, topological superconductors, and axion insulators.[16] Experimental evidence on the nature of 3D Dirac semimetal has been provided from angle-resolved photoemission (ARPES) measurements on either (001) surface[17–20] or the (100) surface of Na_3Bi.[21,22] A clear chiral anomaly is also observed in Na_3Bi.[23] Later on, Cd_3As_2 has been established as another Dirac semimetal both theoretically and experimentally.[26–32]

Here we report comprehensive high-resolution angle-resolved photoemission measurements on the two cleaved surfaces, (001) and (100), of Na_3Bi. On the (001) surface, by comparison with theoretical calculations, we provide a proper assignment of the observed bands, and in particular, pinpoint the band that is responsible for the formation of the three-dimensional Dirac cones. By varying incident photon energies thus varying the out-of-plane k_z values, a pair of separated 3D Dirac nodes are revealed, which locate symmetrically along A–Γ–A direction with respect to Γ. In addition to the single Dirac node at the zone center, we observed six faint point-like Fermi surface at zone corners that may be related with surface reconstruction. On the (100) surface, our ARPES measurements over a large momentum space raise an issue on the selection of the basic Brillouin zone in the (100) plane. We directly observe two isolated 3D Dirac nodes on the (100) surface. We observe the signature of the Fermi-arc surface states connecting the two 3D Dirac nodes that extend to a binding energy of ~150 meV before merging into the bulk band. Our results constitute strong evidence on the observation of three-dimensional Dirac semimetal state in Na_3Bi that are basically consistent with previous theoretical[16] and experimental work.[17,21,22] In addition, our results provide new information to clarify on the nature of the band that forms the 3D Dirac cones, on the possible formation of surface reconstruction of the (001) surface, and on the issue of basic Brillouin zone selection for the (100) surface. The electronic information is important in further study of the topological nature of the three-dimensional Dirac semimetal Na_3Bi.

2. Experimental methods

Angle-resolved photoemission measurements were carried out on our lab ARPES system equipped with the Scienta R4000 electron energy analyzer[46] and by ARPES systems using synchrotron light source. For our Lab ARPES measurements, light sources including vacuum ultraviolet (VUV) laser ($h\upsilon = 6.994$ eV)[46] and He Iα ($h\upsilon = 21.2$ eV, He Iα hereafter) were used, with the corresponding energy resolution set at 1.5 meV and 20 meV, respectively. The angular resolution is ~0.3 degree. Synchrotron radiation ARPES measurements were performed at beamlines BL-1 and BL-7 in Hiroshima Synchrotron Radiation Center (HiSOR), Hiroshima University, Japan. The incident photon energy at BL-1 was varied between 48 and 64 eV and the energy resolution was set at ~15 meV. The incident photon energy at BL-7 was varied from 48 to 116 eV and the energy resolution was set at ~50 meV. The Fermi level is referenced by measuring on a clean polycrystalline gold that is electrically connected to the sample. High-quality single crystals of Na_3Bi were grown by the self-flux method. The atomic ratio of Na to Bi of the grown crystals were measured by Inductively Coupled Plasma Atomic Emission Spectroscopy (ICP-AES) which corresponds to 1 to 0.33 that is consistent with the stoichiometry of Na_3Bi. Since Na_3Bi is extremely sensitive to air, all the sample preparations are carried out in a glove box filled with Argon. Specifically, in order to obtain two cleaving surfaces, i.e., (001) and (100) surfaces, the Na_3Bi samples were cut and pasted along two orthogonal directions. For ARPES measurements, all the samples were cleaved *in situ* in vacuum with a base pressure better than 8.0×10^{-11} mbar and at a temperature of ~25 K.

The electronic structure calculations were performed by using the full-potential augmented plane-wave and Perdew–Burke–Ernzerhof parametrization of the generalized gradient approximation (GGA-PBE) exchange-correlation function[47] as implemented in the WIEN2k code.[48] The spin-orbital interaction is included by using a second variational procedure. The muffin-tin radii RMT is set to be 2.50 bohrs for both Na and Bi. The plane-wave cutoff ($K_{\max}$) is determined by $R_{\min}K_{\max} = 7.0$, where $R_{\min}$ is the minimal RMT. The local density of states (LDOS), from which we can obtain the dispersion of the surface states, is conveniently obtained through the maximally localized Wannier functions derived from the *ab initio* calculations.

3. Results and discussion

3.1. Preparation of two cleaved surfaces (001) and (100) of Na_3Bi and their characterizations

Figure 1 shows basic information and characterization of Na_3Bi. Figure 1(a) shows the crystal structure of Na_3Bi with a space group of $P6_3/mmc$ and the lattice constants $a = b = 5.448$ Å and $c = 9.655$ Å. Figure 1(b) shows the corresponding bulk Brillouin zone, projected (001) surface Brillouin zone (hexagon above the bulk Brillouin zone), and (100) surface Brillouin zone (rectangle in front of the bulk Brillouin zone) of Na_3Bi.

We performed x-ray diffraction (XRD) analysis on the

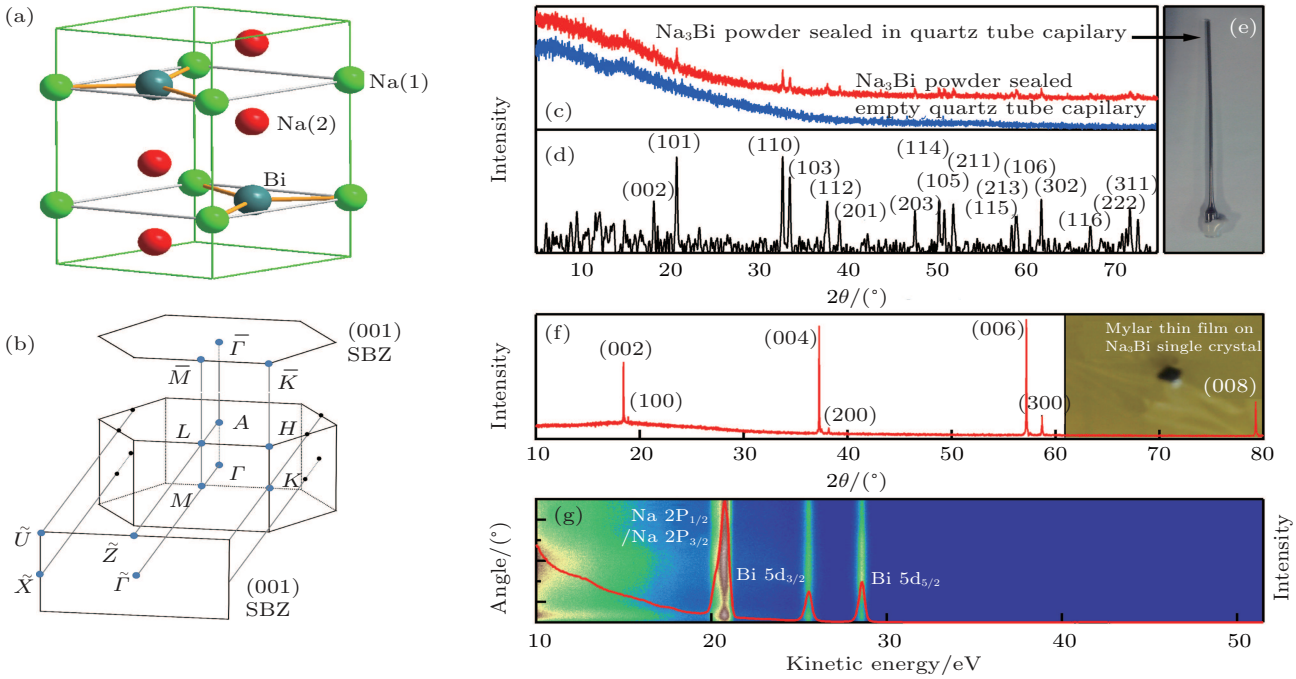


Fig. 1. Basic information of Na_3Bi. (a) Crystal structure of Na_3Bi. It consists of two Na_3Bi units in a unit cell and has an inversion center. (b) Brillouin zones of Na_3Bi. The hexagon and the rectangle are projected surface Brillouin zones of (001) and (100) surface, respectively. (c) XRD measurement on powder Na_3Bi sample which was sealed in an ultra thin quartz capillary shown in panel (e). Red and blue curves are XRD patterns of empty quartz capillary and the quartz capillary with Na_3Bi powder sealed inside, respectively. (d) shows their difference that represents the signal from the Na_3Bi powder sample. (f) XRD pattern on a Na_3Bi single crystal covered with Mylar thin film for protection from air. The right inset shows the picture of the measured sample. (g) Core levels of Na $2P_{1/2}$, Na $2P_{3/2}$ and Bi $5d_{3/2}$, Bi $5d_{5/2}$ in a photoemission spectrum taken with the incident photon energy of 56 eV.

crystal structure of Na_3Bi on both the powder and crystal samples. Since Na_3Bi is very reactive to air, the Na_3Bi powder was put inside a small ultra-thin quartz capillary (mark-tubes made of special glass No. 10, Hilgenberg GmbH, see Fig. 1(e)) for x-ray diffraction analysis. Figure 1(c) shows the x-ray diffraction patterns on an empty quartz capillary (blue curve) and a quartz capillary with Na_3Bi powder sealed inside (red curve). Their difference represents the XRD diffraction signal from the Na_3Bi sample that is shown in Fig. 1(d). The observed peaks can be well identified as the diffraction peaks from Na_3Bi. Figure 1(f) shows XRD diffraction pattern for Na_3Bi single crystal. In this case, the sample was covered with a piece of Mylar thin film (right inset of Fig. 1(f)) to protect it from air. Two groups of peaks can be observed, with the main contribution coming from the (001) surface. The weak peaks of (100) surface may be due to a small deviation of sample orientation or a presence of a small piece of crystal with (100) orientation. We also measured photoemission spectra of Na_3Bi over a wide energy range (Fig. 1(g)). The integrated energy distribution curve (EDC, red curve in Fig. 1(g))) shows the location of the Na 2p core level and the doublet of Bi 5d core level.

Since the confirmation of three-dimensional Dirac cones needs to have access to all three-dimensional Brillouin zone, it is ideal to have ARPES measurements on multiple cleaved surfaces. In Fig. 2, we show our approach to obtain two cleaved surfaces (001) and (100) of Na_3Bi *in situ* in vacuum. We first chose a piece of high-quality Na_3Bi single crystal and cut it along two orthogonal directions as sketched in Fig. 2(a). As marked by white arrows in Figs. 2(b) and 2(c), the obtained cleaved (001) surface (Fig. 2(b)) and (100) surface (Fig. 2(c)) are flat and shiny. Figures 2(d) and 2(e) illustrate surface atomic structures of the (001) and (100) surfaces, respectively. We carried out Fermi surface mapping measurements over a large momentum space on these two kinds of Na_3Bi samples; the observed three-fold symmetry in Fig. 2(f) and the mirror symmetry in Fig. 2(g) are consistent with the cleaved surfaces being (001) and (100) surfaces, respectively.

3.2. ARPES on the (001) surface of Na_3Bi

The access of three-dimensional Brillouin zone in studying the Dirac nodes in Na_3Bi asks for a precise determination of momentum for each ARPES measurement. While it is straightforward to determine the in-plane momentum because it is conserved during the photoemission process, the determination of the out-of-plane component is tricky. Since the photo-emitted electrons have to overcome a potential barrier (inner potential V_0) before they escape from the sample surface, the determination of the out-of-plane momentum requires the value of V_0 beforehand. The k_z can then be determined from the incident photon energy ($h\nu$) and the emission angle θ by taking the formula[49]

$$k_z = 1/\hbar\sqrt{2m[(h\nu - W - E_b)\cos^2\theta + V_0]}, \qquad (1)$$

where W is the work function, E_b denotes the binding energy, θ is the angle between the emission direction and the sample

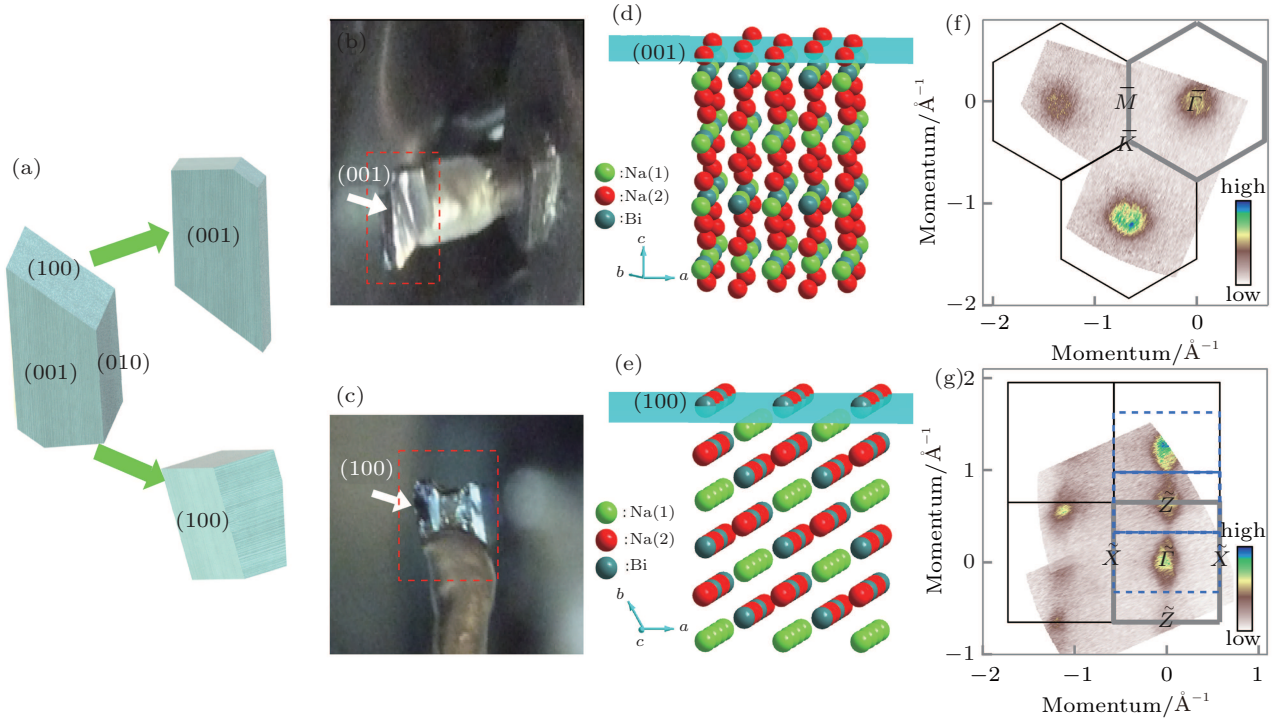


Fig. 2. Intentional cleavage of the (001) and (100) surfaces of the Na_3Bi crystals. (a) Sketch of the intentional cutting process of the Na_3Bi single crystal to cleave at the desired (001) and (100) surfaces. (b) Photo of the cleaved (001) surface taken after ARPES measurements. (c) Photo of the cleaved (100) surface taken after ARPES measurements. (d) Schematic atomic structure of the (001) surface. (e) Schematic atomic structure of the (100) surface. (f) Large momentum space Fermi surface mapping on the (001) surface of Na_3Bi using 21.2 eV photon energy. (g) Large momentum space Fermi surface mapping of the (100) surface of Na_3Bi using 21.2 eV photon energy.

normal direction. The k_zs for a given photon energy form a curved surface in momentum space which is related to different emission angles θ of the photoelectrons. For simplicity and to avoid ambiguity, the k_z we mention below refers to the value for the normal direction photoemission.

The inner potential V_0 of the Na_3Bi (001) surface can be determined from ARPES measurements on the (001) surface by varying the phonon energy (see Fig. 3). Figure 3(a) shows photoemission spectra (EDCs) taken along the sample normal direction at various photon energies between 40 eV and 116 eV. Figure 3(b) presents a two-dimensional image that shows the photoemission intensity as a function of the binding energy and the incident photon energy for the normal emission. From Figs. 3(a) and 3(b), focusing on the bands at $E_b \sim 2.0$ eV and $\sim$1.0 eV, it is obvious that the repetition appears around 56 eV and 101 eV which correspond to two Γ points along the Γ-A direction. By using Eq. (1), taking $c' = 0.5c = 0.5 \times 9.655$ Å = 4.8275 Å as we will explain below, the inner potential V_0 for the (001) surface of Na_3Bi is estimated to be around 9.0 eV (sensitively depends on the determination of the repeated photon energies).

Figure 4 presents the Fermi surface and band structures taken on the (001) surface of Na_3Bi measured by lab ARPES system with a photon energy of 21.2 eV. In Fig. 4(a), we sketch the two three-dimensional Dirac nodes located near the Γ point along the Γ–A line in the bulk Brillouin zone, as expected for Na_3Bi from theoretical calculations.[16] The projection of the 3D bulk Dirac nodes to the surface Brillouin zones at the (001) and (100) surface are also shown. The red dashed line connecting the two Dirac cones for the (100) surface represents topological nontrivial surface state with arc structure.[16] The atomic structures of both (001) and (100) surfaces are also drawn in Fig. 4(a). The 3D Dirac nodes are predicted to be located at $\pm k_{zc}$ ($k_{zc} = 0.085$ Å^{-1}) along A–Γ–A direction in Na_3Bi (Fig. 4(a)). The k_z value estimated for the photon energy of 21.2 eV, taking $V_0 \sim 9.0$ eV as determined before, is around 0.02 Å^{-1}. This is quite close to the value of k_{zc}, especially when considering the finite momentum resolution along the k_z direction. Therefore, He Iα with 21.2 eV photon energy is suitable to probe the 3D Dirac nodes on the (001) surface of Na_3Bi.

Figure 4(b) presents the Fermi surface of Na_3Bi over a large momentum space that covers both the first and second hexagonal surface Brillouin zones of the (001) surface. The repetition of the strong signal near the three Γ points is consistent with the (001) surface. Figure 4(c) shows the band structure measured along the $\bar{\Gamma}\bar{M}$ direction, where six bands can be well resolved and labeled in sequence from the Fermi level to high binding energy by α, β, γ, δ, ε, and ζ. For comparison, the calculated result with the same energy scale and momentum direction with $k_z = 0.02$ Å^{-1} is also presented in Fig. 4(d). Within experimental uncertainness, the measured band structures in Fig. 4(c) show a perfect match with the calculated result in Fig. 4(d). From Figs. 4(c) and 4(d), also from more results below, it is clear that the spot-like Fermi surface

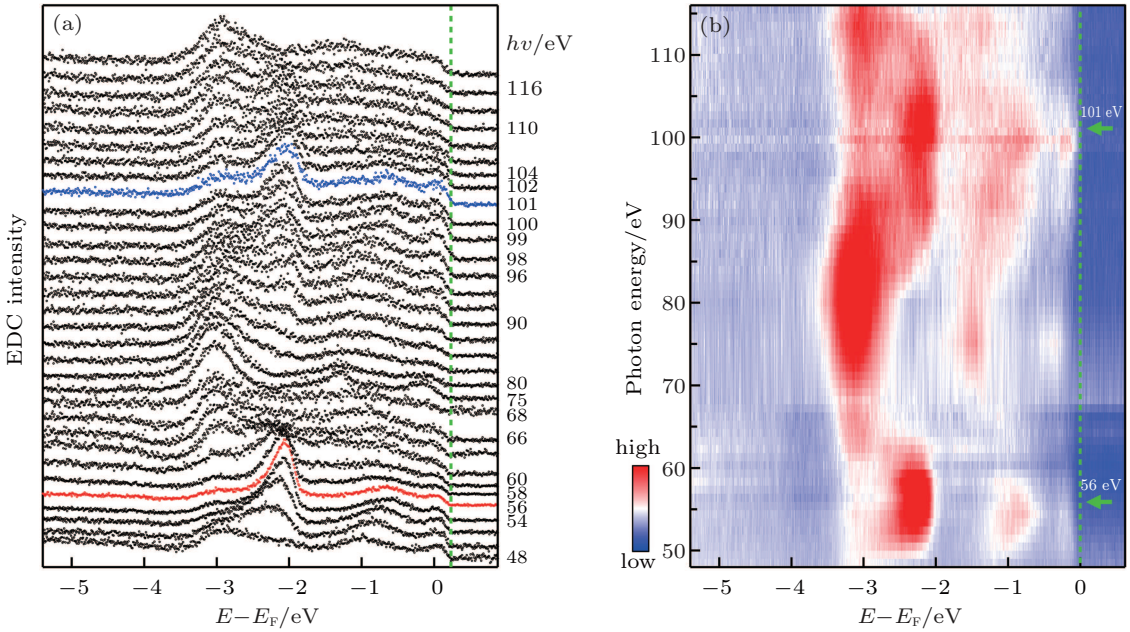


Fig. 3. Normal emission photoemission spectra (EDCs) measured on the (001) surface of Na_3Bi at different photon energies. (a) Normal emission EDCs taken with different incident photon energies from 48 eV to 116 eV. Red and blue colored EDCs with incident photon energies of 56 eV and 101 eV represent a repetition period that cover a complete Brillouin zone along k_z direction. (b) The corresponding EDC stacking image of panel (a) with proper normalization and interpolation. Apparently, the band repeats around photon energies of 56 eV and 101 eV as highlighted in both panels (a) and (b). The inner potential V_0 is thus estimated to be around 9.0 eV.

feature at the zone center in Fig. 4(b) originates from the bulk band α, which is linearly dispersive near the Fermi level and forms the three-dimensional Dirac cones.

In order to verify the Dirac cone structure formed by the α band, we take fine Fermi surface mapping of the (001) surface in the first surface Brilouin zone as shown in Fig. 4(e). The spot-like Fermi surface at the zone center is the Dirac point since the Fermi level of the freshly cleaved sample is just pinned at the Dirac point. Figure 4(f) shows the detailed band structure evolution around the $\bar{\Gamma}$ point. In the energy range between the Fermi level and a binding energy of 0.8 eV, only α and β bands are observed as shown in Fig. 4(f). When the momentum cut is right across the $\bar{\Gamma}$ point (cut 4 in Fig. 4(e)), the α band in Fig. 4(f4) just crosses the point and shows a linear dispersion over an energy range of ~0.5 eV. When the momentum cuts move away from the $\bar{\Gamma}$ point, the top position of the α band sinks below the Fermi level and can be well described by the hyperbolic cone-shaped curves as shown by the dotted lines. Such a momentum evolution of the band structures confirms the Dirac cone-like structure of the α band. For a 3D Dirac cone with the Dirac nodes at Fermi level, it usually has the form $E = \pm\sqrt{a_x^2(k_x-b_x)^2 + a_y^2(k_y-b_y)^2 + a_z^2(k_z-b_z)^2}$. Here, $a_{x,y,z}$ are associated with the cone shape (slope of the cut across the generatrix of the projected 2D gapless cone) and $b_{x,y,z}$ are the momentum loci of the 3D Dirac nodes in the Brillouin zone. The cone shape of the α band on the (001) surface of Na_3Bi can be well reproduced by fitting parameters $a_x = a_y = \sim 1.5$ eV·Å, $b_x = b_y = 0$ Å^{-1}, regardless of the very small contribution of the k_z direction.

Our observation of a Dirac cone on the (001) surface of Na_3Bi and the corresponding momentum dependence show some overall resemblance to the previous results.[17] However, we note that there appears to be a difference on the exact band that forms the Dirac cones. In our measurements, the α band is strong and is the origin of the Dirac cone. This is consistent with the theoretical calculations which indicate that it is the topmost band α below the Fermi level that forms the 3D Dirac cone.[16] However, we note that the intensity of α band in the previous measurements[17] is rather weak probably due to photoemission matrix element effect under different measurement conditions. The difference could be quantitatively determined and shown by the Dirac cone shape fitting parameters which have values of ~ 1.5 eV·Å in our case, in contrast to those of ~ 2.5 eV·Å in the previous measurement.[17] In this case, which band forms the purported Dirac cones needs to be further checked.[17]

In order to explore the two 3D Dirac nodes separated along the A–Γ–A direction as sketched in Figs. 4(a) and 5(a), we measured the band structures of the Na_3Bi (001) surface at different out-of-plane k_zs with different photon energies by using synchrotron radiation ARPES, as shown in Fig. 5(c), with the photon energies used and the corresponding k_zs marked. In Fig. 5(c), the dashed red lines are fitted to the α band according to the Dirac cone shape. The linearly dispersive band touches the Fermi level at the photon energy of 53.3 eV and moves away from the Fermi level with further increase of the photon energy. It touches the Fermi level again at the photon energy of 58.4 eV and sinks below the Fermi level with the further increase of the photon energy.

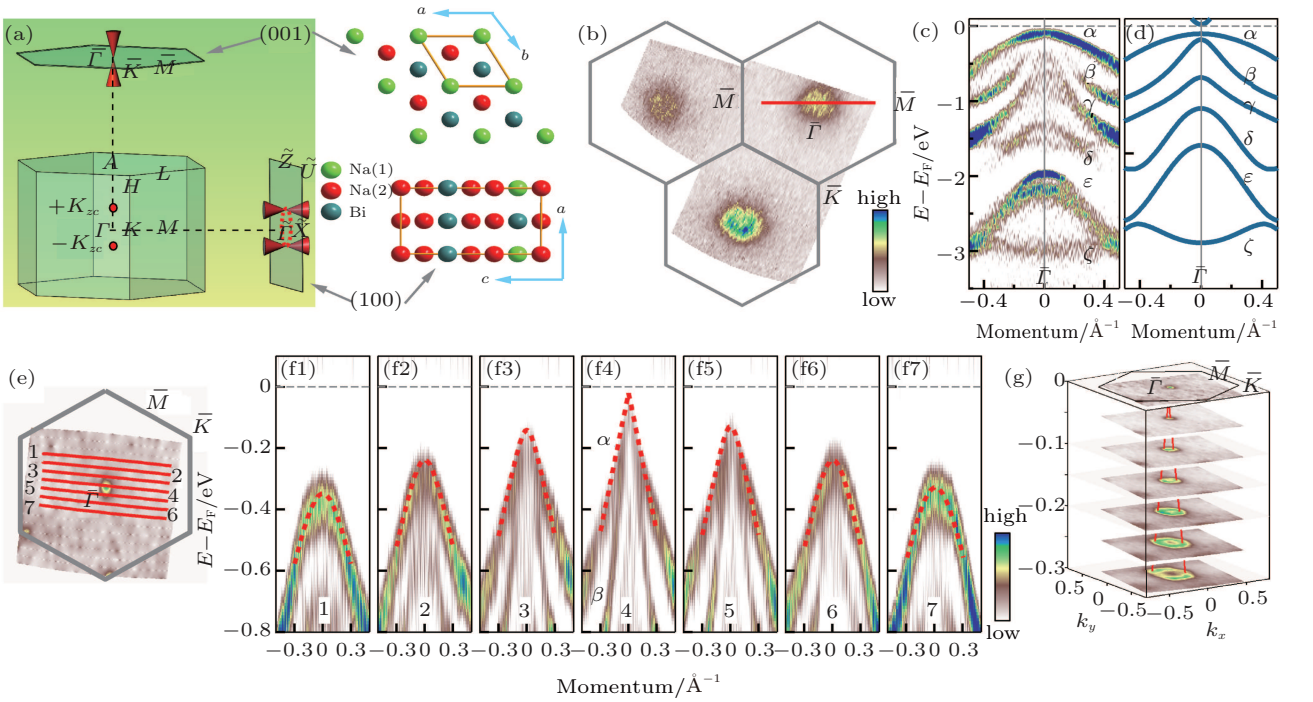


Fig. 4. Fermi surface and band structures taken on the (001) surface of Na_3Bi by using He Iα (21.2 eV) light source. (a) Sketch of the momentum position of the 3D bulk Dirac nodes in the bulk Brillouin zone and their projections onto the surface Brillouin zones on the (001) and (100) surfaces. The red dashed line connecting the two Dirac cones on the (100) surface represents nontrivial surface state with an arc structure. The atomic structures of both the (001) and (100) surfaces are also drawn. (b) Fermi surface covering a large momentum space of the first and second Brillouin zones on the (001) surface. (c) Band structure along the $\bar{M}$–$\bar{\Gamma}$–$\bar{M}$ momentum cut as marked by a red line in (b). (d) Calculated band structure along the same momentum cut as (c). (e) Fine mapping of the Fermi surface around the $\bar{\Gamma}$ point on the (001) surface. (f) Band structures measured along seven momentum cuts labeled as red lines 1 to 7 in panel (e). The red dashed lines are fitted curves considering the Dirac cone shape. (g) Three-dimensional view of the evolution of Fermi surface and constant energy contours at different binding energies. The red lines are the guide to the eye. The band images are all obtained by the second derivative of the original data with respect to the energy.

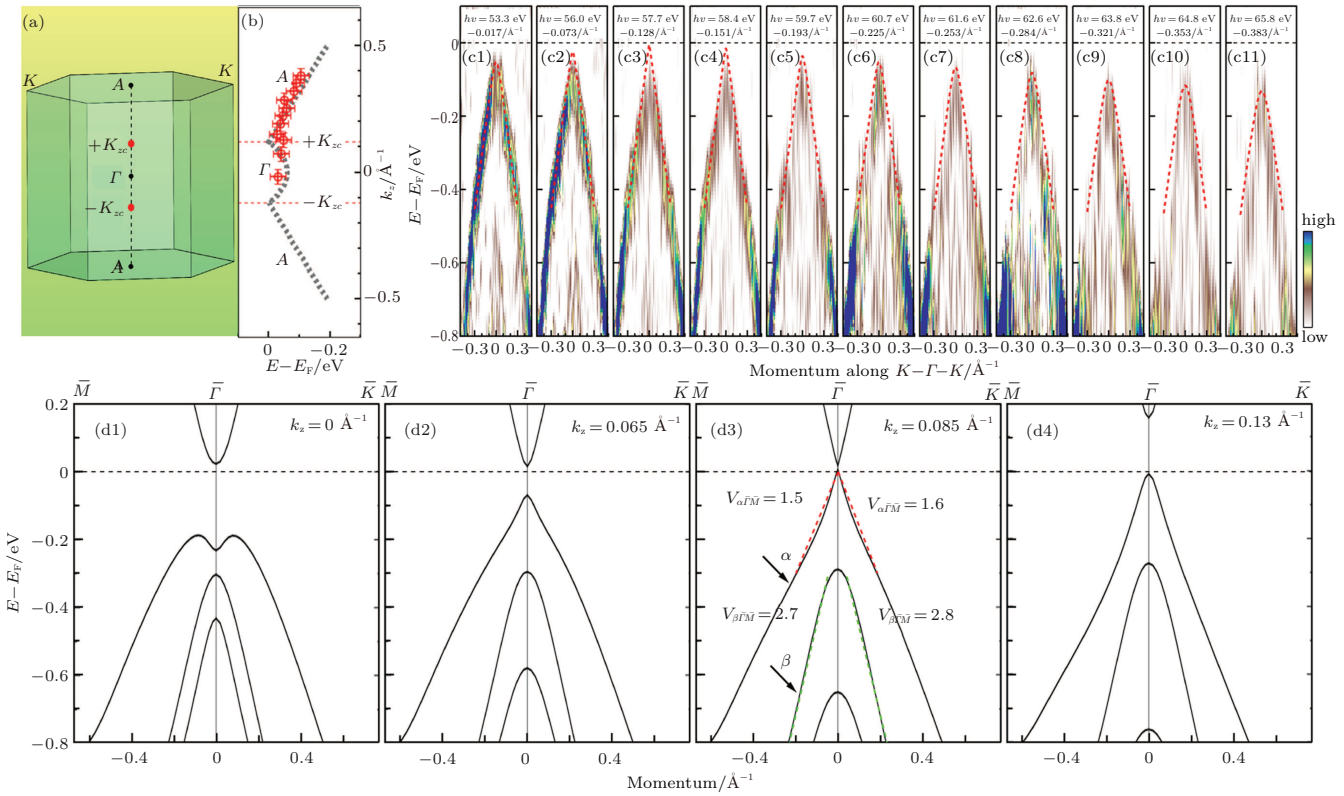


Fig. 5. Detection of the two three-dimensional Dirac cones along the k_z direction. (a) The sketch of the bulk Brillouin zone of Na_3Bi. Two three-dimensional bulk Dirac nodes are labeled as $+k_{zc}$ and $-k_{zc}$ along the A–Γ–A direction. (b) The extracted energy position of the α band top as a function of k_z calculated from different photon energies shown in panel (c). The gray dashed line is the guide to eyes. (c) Band structures measured on the (001) surface of Na_3Bi along $\bar{K}$–$\bar{\Gamma}$–$\bar{K}$ direction at different photon energies. The images are obtained by taking EDC second-derivative of the original data. The red dashed lines are fitted curves considering the Dirac cone shape. (d) Calculated band structure along $\bar{M}$–$\bar{\Gamma}$–$\bar{K}$ direction at different k_zs. The bands at a critical k_{zc} in (d3) show a Dirac point. The slopes of α and β bands are around 1.5 eV·Å and 2.7 eV·Å, respectively.

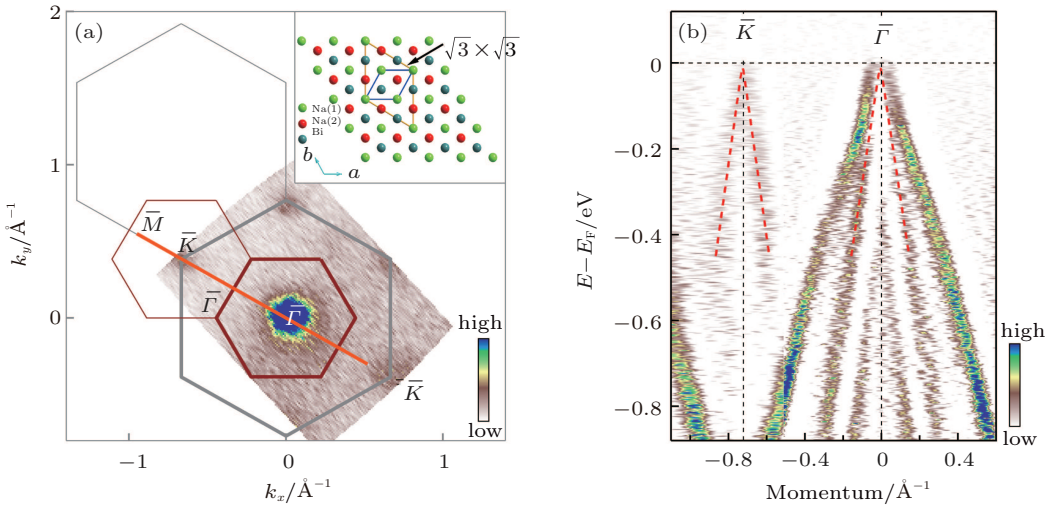


Fig. 6. Fermi surface and band structures taken by the photon energy of 21.2 eV around the $\bar{K}$ points on the (001) surface of Na_3Bi. (a) Observation of features around the $\bar{K}$ points. The upper-right inset image is the projection view of the (001) surface atomic structure. The blue rhombus and the orange rhombus show the repetition unit cells of the surface, where the length of the unit vector of the orange rhombus is $\sqrt{3}$ times that of the red one. While the small blue rhombus corresponds to a large surface Brillouin zone as a gray hexagon, the expanded orange rhombus corresponds to the smaller surface Brillouin zone marked as a red hexagon. The possible $\sqrt{3}\times\sqrt{3}$ surface reconstruction makes the original six $\bar{K}$ points equivalent to the $\bar{\Gamma}$ point. This gives rise to a possible band folding of the bands near $\bar{\Gamma}$ point to the $\bar{K}$ points. (b) Band structure measured along $\bar{M}$–$\bar{K}$–$\bar{\Gamma}$–$\bar{K}$ as indicated by a orange line in panel (a). It is obtained by second derivative of the original data with respect to momentum direction. The band slope near the Fermi level at both $\bar{\Gamma}$ and $\bar{K}$, which are fitted with red dashed linear lines, are similar with an estimated value around 3.0 eV·Å.

The photon-energy-dependent band dispersions in Fig. 5(c) clearly indicate the 3D nature of the Dirac points in Na_3Bi. With the estimated inner potential of ~9 eV for the (001) surface of Na_3Bi, we can calculate the value of the k_z for each incident photon energy with Eq. (1).[49] Meanwhile, we pick up the binding energy of the top of the α band in Fig. 5(c) and plot them as a function of the related k_z in Fig. 5(b), where the red circles represent the experimental data and the light gray dashed line is the guide to the eye. The k_z value associated with the photon energy of 56 eV is very close to one of the unique momentum k_{zc} located at $+0.085$ Å^{-1} along A–Γ–A direction. Although there is a slight deviation of the experimental data from the theoretically expected values due to the inherently limited k_z resolution of the ARPES measurements, one can see a nearly linear dispersion along the k_z direction between k_{zc} and point A. In between the two k_{zc} momentum points, the dispersion deviates from the expected linear dispersion due to the hybridization of the two bulk Dirac cones, which are located very close to each other along the k_z direction. The gray dashed line approximately tracks the α band dispersion along A–Γ–A direction which gives the rest 3D Dirac cone parameters in the k_z direction by a_z=~ 0.5 eV·Å and b_z= ~ ±0.12 Å^{-1}. Figure 5(d) shows the evolution of the calculated bands with k_z. Note that the upper-most α band is responsible for the 3D Dirac cone formation, with a dispersion slope around 1.5 eV·Å at the Dirac point (Fig. 5(d3)), which is flatter than the β band with a slope near 2.7 eV·Å (Fig. 5(d3)). The slopes of the α and β bands provide us another way to determine the band that forms the 3D Dirac cone. The slopes of our observed α and β bands in Figs. 4(f) and 5(c) are consistent with the calculated results (Fig. 5(d3)). The linear dispersive of the α band along the out-of-plane k_z direction, together with the results in the k_x–k_y plane in Fig. 4, constitute overall evidence of the linear dispersion of the Dirac fermions along all the three momentum directions that unambiguously establishes the existence of the 3D bulk Dirac cones in Na_3Bi, with a set of parameters given by $a_x = a_y$ =~ 1.5 eV·Å, a_z =~ 0.5 eV·Å and $b_x = b_y = 0$ Å^{-1}, b_z =~ ±0.12 Å^{-1}.

Upon careful examination, we find that there are Dirac-cone-like structures forming spot-like Fermi pockets around the $\bar{K}$ points on the (001) surface of Na_3Bi (Fig. 6(a)). Figure 6(b) shows the band structure measured along the $\bar{M}$–$\bar{K}$–$\bar{\Gamma}$–$\bar{K}$ line as indicated by the orange line in Fig. 6(a). The intensity of the bands around the $\bar{K}$ point is much weaker than that around the $\bar{\Gamma}$ point, but their presence is quite clear. Near the Fermi level, the slope of the bands around the $\bar{K}$ points is similar to that of the β band around the $\bar{\Gamma}$ point, as highlighted as red dashed lines in Fig. 6(b). From the band structure calculations on Na_3Bi, there is a band gap about 1 eV near $\bar{K}$ point and there are no surface states there.[16] The origin of the feature near $\bar{K}$ points needs to be further studied. One possibility is that the features near $\bar{K}$ points are due to folding of the bands near $\bar{\Gamma}$ point. This implies that there is a surface reconstruction on the (001) surface. According to the symmetry of the Fermi surface features around the $\bar{K}$ points, the (001) surface with a $\sqrt{3}\times\sqrt{3}$ reconstruction (inset of Fig. 6(a)) and the corresponding shrunk Brillouin zone (red thick hexagon around $\bar{\Gamma}$ in Fig. 6(a)) could be consistent with the observations.

3.3. ARPES on (100) surface of Na_3Bi

Besides the 3D bulk Dirac nodes, the topological nontrivial surface-state Fermi arcs connecting the two 3D bulk Dirac nodes is another significant and peculiar feature of the Dirac semimetal Na_3Bi.[16] As shown in Fig. 4(a), ARPES measurements taken on the (100) surface will be able to directly and simultaneously reveal a pair of the 3D bulk Dirac nodes as well as the nontrivial surface state Fermi arcs between them, thus capturing the main and most important physics of Dirac semimetal. We managed to *in situ* cleave the Na_3Bi single crystal samples to obtain the (100) surface, as shown in Fig. 2. We also carefully tuned the incident photon energy to vary the out-of-plane k_y momentum in order for ARPES to detect the 3D bulk Dirac nodes at the momentum position with $k_y = 0$. One suitable incident photon energy we find is ~56 eV.

Figure 7 shows the measured Fermi surface and the constant energy contours (CECs) at different binding energies on the (100) surface of Na_3Bi taken with a photon energy of 56 eV. The coverage of large momentum area allows us to find the repetition unit in the reciprocal space. From the crystal structure shown in Fig. 1(a) with lattice constants $a = b = 5.448$ Å and $c = 9.655$ Å, the corresponding unit cell of the (100) surface Brillouin zone should be a rectangle (Fig. 1(b)) with $a' = 1.15$ Å^{-1} and $c' = 0.65$ Å^{-1}, as shown by a blue dashed rectangle in Fig. 7(a). It is clear that such a unit cell cannot explain our measured data (Fig. 7), particularly along the k_z direction. In order to explain the periodicity of the observed data, we have to expand the unit cell length along the k_z direction twice so that $a' = 1.15$ Å^{-1} and $c'' = 2 \times 0.65 = 1.3$ Å^{-1}, as shown by the solid grey rectangle in Fig. 7(a). This new unit cell can basically explain the periodicity of our observed results. In this case, the intensity in the first and third Brillouin zones are much stronger than that in the second zones. This may be due to the photoemission matrix element effect.

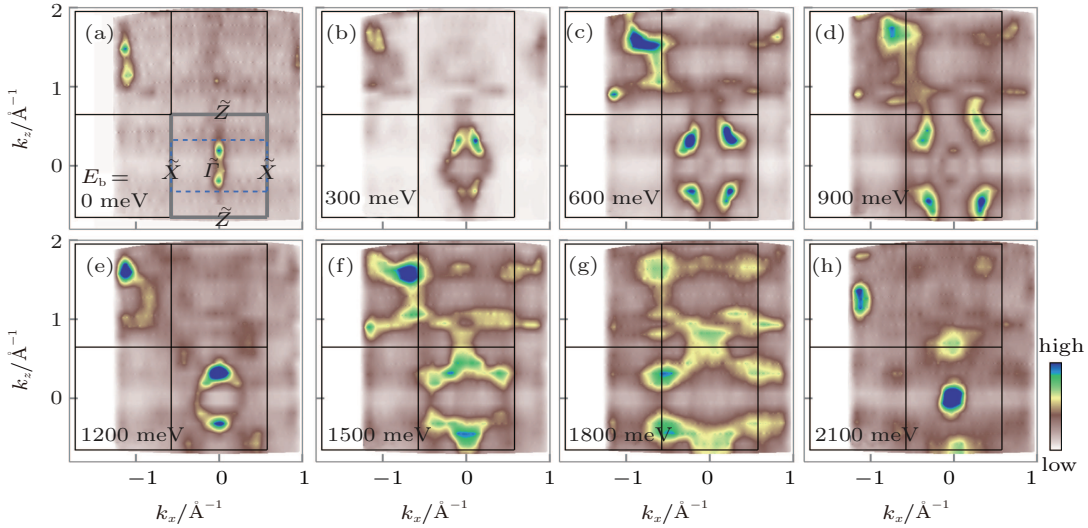


Fig. 7. Fermi surface and constant energy contours at different binding energies taken by 56 eV photons on the Na_3Bi (100) surface. (a) Two pairs of node-like Fermi surfaces along $\widetilde{Z}$–$\widetilde{\Gamma}$–$\widetilde{Z}$. The blue dashed rectangle is the (100) surface Brillouin zone derived directly from the crystal structure of Na_3Bi (Fig. 1(a)). The thick gray rectangle is the surface Brillouin zone defined by the results of the constant energy contours. In this case, the unit cell of the surface Brillouin zone is doubled along the $\widetilde{Z}$–$\widetilde{\Gamma}$–$\widetilde{Z}$ direction while it remains the same along the $\widetilde{X}$–$\widetilde{\Gamma}$–$\widetilde{X}$ direction. (b)–(h) Constant energy contours at different binding energies taken on the (100) surface of Na_3Bi.

We further examine the issue of the surface Brillouin zone on the (100) surface of Na_3Bi by checking on the band structures, as shown in Fig. 8. Figures 8(a) and 8(b) are Fermi surfaces taken with photon energies of 56 eV and 21.2 eV, respectively. Figures 8(c) and 8(d) are band structures taken along the $\widetilde{Z}$–$\widetilde{\Gamma}$–$\widetilde{Z}$ momentum cut marked by gray lines in Figs. 8(a) and 8(b), respectively. From the spectral weight distribution in the Fermi surface (Fig. 8(a)) and the band structure along the $\widetilde{Z}$–$\widetilde{\Gamma}$–$\widetilde{Z}$ momentum cut (Fig. 8(c)) measured at 56 eV photon energy, it is clear that there is a periodicity along k_z direction that is twice of the original $c' = 0.65$ Å^{-1} defined by real space unit cell in Fig. 1(a), i.e., $c' = 2 \times 0.65 = 1.3$ Å^{-1} as shown by the thick grey rectangle in Fig. 8(a). The overall band evolution from e1 to e5 cuts (Fig. 8(e)) and from f1 to f5 cuts (Fig. 8(f)) is consistent with this assignment. Similar band structures measured along e1 cut (Fig. 8(e1)) and g1 cut (Fig. 8(g1)), and along e2 cut (Fig. 8(e2)) and g2 cut (Fig. 8(g2)), also support this picture. This double-k_z periodicity is also clear in the Fermi surface (Fig. 8(b)) and the band structure along the $\widetilde{Z}$–$\widetilde{\Gamma}$–$\widetilde{Z}$ momentum cut (Fig. 8(d)).

However, by examining the band structures measured at 56 eV and the Fermi surface measured at 21.2 eV (Fig. 8(b)), there seems to be another period that agrees with the original unit cell defined by the real space crystal structure in Fig. 1(a). Looking at the measured band structures carefully along e1 cut (Fig. 8(e1)) and e2 cut (Fig. 8(e2)), there are clear bands that are marked by α' (red dashed lines in Fig. 8(e)) and γ' (blue dashed lines in Fig. 8(e)) although their intensity is

strongly suppressed. Considering the presence of these α' and γ' bands, one may see the similarity of band structures between (e1-e5) cuts and (f1-f5) cuts. This is consistent with a smaller weak period along k_z direction with a normal value of π/c (dashed blue rectangular). The spectral weight distribution in the Fermi surface mapping measured at 21.2 eV (Fig. 8(b)) is also consistent with the presence of this weak period that has a normal unit cell expected from real space crystal structure in Fig. 1(a).

We note that there is a controversy in the literatures regarding the selection of the basic Brillouin zone in the k_x–k_z (100) plane.[17,22] From an indirect photon energy dependent measurement on the (001) surface, the size of (100) surface Brillouin zone is used, which is derived directly from the real space crystal structure with $a' = 1.15$ Å^{-1} and $c' = 0.65$ Å^{-1}.[17] In another direct measurement on the (100) surface of Na_3Bi, a much large Brillouin zone unit cell is used, which expands the length twice along both k_x and k_z directions, i.e., $a' = 1.15 \times 2 = 2.3$ Å^{-1} and $c' = 0.65 \times 2 = 1.3$ Å^{-1}.[22] In our case of direct ARPES measurements on (100) surface of Na_3Bi over a large momentum space, we find there is a strong period and a weak period along k_z direction. For the strong period, we need to double the length along k_z direction, while keep the length along the k_x direction intact, i.e., $a' = 1.15$ Å^{-1} and $c' = 0.65 \times 2 = 1.3$ Å^{-1}. Such a Brillouin zone doubling along k_z direction is not present in the theoretical calculations; it is also different from the previous results.[17,22] The expansion of the Brillouin zone is unusual because in most cases one would see the shrinkage of the Brillouin zone due to real space structural reconstruction that leads to expansion of unit cell size in the real space. The origin of the reciprocal space unit cell expansion in Na_3Bi needs further investigation. One possibility may be related with the presence of an inversion center in Na_3Bi which makes the two Na_3Bi layers in one unit cell equivalent, as seen in Fig. 1(a). On the other hand, we also show the signature of a weak period that is consistent with the normal unit cell expected from the real space crystal structure of Na_3Bi (Fig. 1(a)).

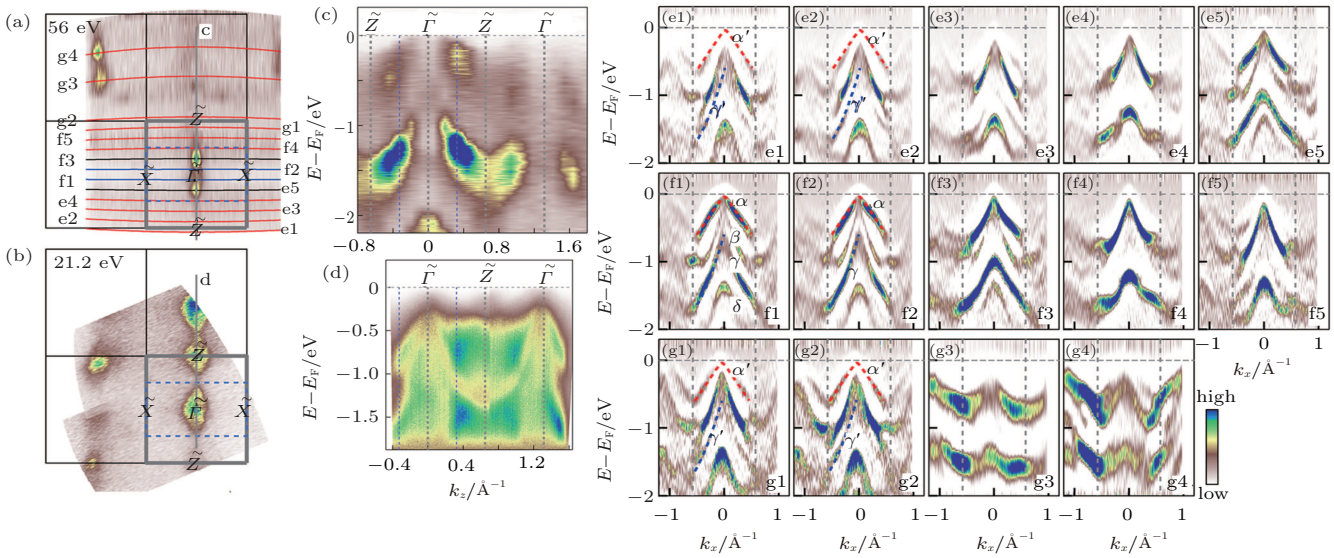


Fig. 8. Detailed band structures of Na_3Bi measured on the (100) surface. (a) Fermi surface taken on the (100) surface with a photon energy of 56 eV. (b) Fermi surface taken on the (100) surface by using He Iα (21.2 eV) light source. (c) Band structure along $\widetilde{Z}$–$\widetilde{\Gamma}$–$\widetilde{Z}$ line in (a). (d) Band structure along the $\widetilde{Z}$–$\widetilde{\Gamma}$–$\widetilde{Z}$ line in (b). (e)–(g) Band structures measured along the momentum cuts shown as red lines in panel (a). (e1)-(e2) Band structures measured along the e1 and e2 momentum cuts near the lower $\widetilde{Z}$ point in the first Brillouin zone. Weak bands can be observed that are marked by red and blue dashed lines and labelled as α' and γ'. They show resemblance to the α and γ bands in the band structure around $\widetilde{\Gamma}$ ((f1), (f2)). (e5) Band structure along a momentum cut that roughly crosses the lower node in the first Brillouin zone. (f1), (f2) Band structures along momentum cuts that are around $\widetilde{\Gamma}$ in the first surface Brillouin zone. Four bands are observed below the Fermi level marked as α, β, γ and δ in sequence. (f3) Band structure along a cut that approximately crosses the upper node in the first surface Brillouin zone. (g1), (g2) Band structures along the cuts around the upper $\widetilde{Z}$ point. Weak bands are observed that are marked by α' and γ'. (g3), (g4) Band structures along cuts that roughly cross nodes in second and third surface Brillouin zones. From panels (e1)–(g2), the major period of (100) projected surface Brillouin zone along $\widetilde{Z}$–$\widetilde{\Gamma}$–$\widetilde{Z}$ is marked by the gray rectangle with an unusual value $\pi/c' = \pi/(0.5c)$. Signature of the small period that is consistent with the usual value π/c as marked by the dashed blue rectangle has also been observed. (g3), (g4) confirm the major period along $\widetilde{Z}$–$\widetilde{\Gamma}$–$\widetilde{Z}$ and provide evidence of the unchanged (100) projected surface Brillouin zone period along $\widetilde{X}$–$\widetilde{\Gamma}$–$\widetilde{X}$.

Figure 9(a) presents the Fermi surface near the zone center measured with a photon energy of 56 eV on the (100) surface of Na_3Bi. Two strong spots located around ± 0.15 Å^{-1} (close to $k_{zc} = \pm 0.085$ Å^{-1}) along $\widetilde{Z}$–$\widetilde{\Gamma}$–$\widetilde{Z}$ (the same as A–Γ–A when $k_y = 0$) direction are observed with a mirror symmetry with respect to the $\widetilde{\Gamma}$ point, which are very close to the position of the 3D bulk Dirac nodes. This is similar to that reported before on the (100) surface of Na_3Bi.[22] These indicate that the observed two spots are associated with the two 3D bulk Dirac nodes on the k_x–k_z plane with $k_y = 0$, as schematically shown in Fig. 4(a). In order to further demonstrate that these two spot-like features are from 3D bulk Dirac nodes, we

examine the band structures carefully by making dense momentum cuts cover the two points, as shown in Fig. 9(c). In the energy range between the Fermi level and a binding energy of 1 eV, two bands of α band and β can be observed. The α bands are fitted with the Dirac cone shape indicated by the dashed red lines. It exhibits a clear linear dispersion when the momentum cut approaches the Dirac nodes (panel 3 in Fig. 9(c) and panel 6 in 9(c)). The slope parameter is found to be $a_x =\sim 1.5$ eV·Å. From a symmetrical view, it is natural to derive $a_x = a_y =\sim 1.5$ eV·Å. The momentum evolution of the band structures along the k_z direction confirms the simultaneous observation of the two 3D bulk Dirac nodes that are located along the A–Γ–A direction with a mirror symmetry with respect to the Γ point of the bulk BZ. Figure 9(b) plots the energy position of the top α band from panels 1–8 in Fig. 9(c) (red circles) as a function of k_z, with the dashed line as the guide to eyes. The linear dispersion of the Dirac bands along k_z and the overall M-shaped curve in Fig. 9(b) are similar to that shown in Fig. 5(b) which have the same quantities measured by two different approaches, i.e., $a_z =\sim 0.5$ eV·Å, $b_z = \pm 0.15$ Å^{-1} (small deviation from ± 0.12 Å^{-1}). Their consistency again confirms the observation of a pair of 3D bulk Dirac nodes along the A–Γ–A direction, with a set of parameters by $a_x = a_y =\sim 1.5$ eV·Å, $a_z =\sim 0.5$ eV·Å, and $b_x = b_y = 0$ Å^{-1}, $b_z =\sim \pm 0.15$ Å^{-1} (small deviation from that of (001) surface with $b_z =\sim \pm 0.12$ Å^{-1}).

In order to resolve the topological nontrivial surface states that connect the two 3D bulk Dirac nodes, we examine the band structures along $\widetilde{X}$–$\widetilde{\Gamma}$–$\widetilde{X}$ direction measured on the (100) surface of Na_3Bi. The band structure obtained by the VUV laser-based ARPES[46] is presented in Figs. 10(a1) and 10(b1) with their second derivative images with respect to the energy shown in Figs. 10(a2) and 10(b2), respectively. As seen more clearly from Fig. 10(b2), there are three main band features where the weaker one crosses the Fermi level, and a stronger one (labeled as α band) and a weaker one (labeled as β band) are below the Fermi level. A close examination on the band near the Fermi level (Figs. 10(a1) and 10(a2)) indicates two branches of a sharp band dispersing linearly from a binding energy of ∼150 meV and crosses the Fermi level. These observations are rather consistent with the band structure calculations (Fig. 10(g)). In this case, the band that crosses the Fermi level is assigned to be the surface state that is predicted for the (100) surface and forms an arc-shaped Fermi surface, as labeled by SS with gray dash guide lines in Figs. 10(a1), 10(a2), 10(b1) and 10(b2). To further verify the surface state nature of the SS band, we performed photon-energy-dependent ARPES measurements with synchrotron radiation light source, as shown in Figs. 10(c)–10(f). The SS band, highlighted by the gray dashed lines, shows little change with the photon energy in terms of the band slope and the Fermi momentum. On the other hand, the other bulk bands, marked by red arrows and black dashed lines, exhibit clear photon energy dependence. These photon-energy-dependent measurements again demonstrate the surface state nature of the SS band on the (100) surface.

We note that there is a sample aging effect during the ARPES measurements of Na_3Bi, on both (100) surface and (001) surface. Figure 11 shows the effect of the sample aging on the measured Fermi surface and band structures of the (100) surface. For the fresh (100) surface of Na_3Bi, a Fermi surface with two clear nodes is clearly observed (Fig. 11(a)). The band along $\widetilde{X}$–$\widetilde{\Gamma}$–$\widetilde{X}$ across the $\widetilde{\Gamma}$ point (Fig. 11(c)) is below the Fermi level. However, after about 2 hours in vacuum, the sample gets aged and measured Fermi surface shows a single hole-like piece (Fig. 11(b)). The corresponding band across

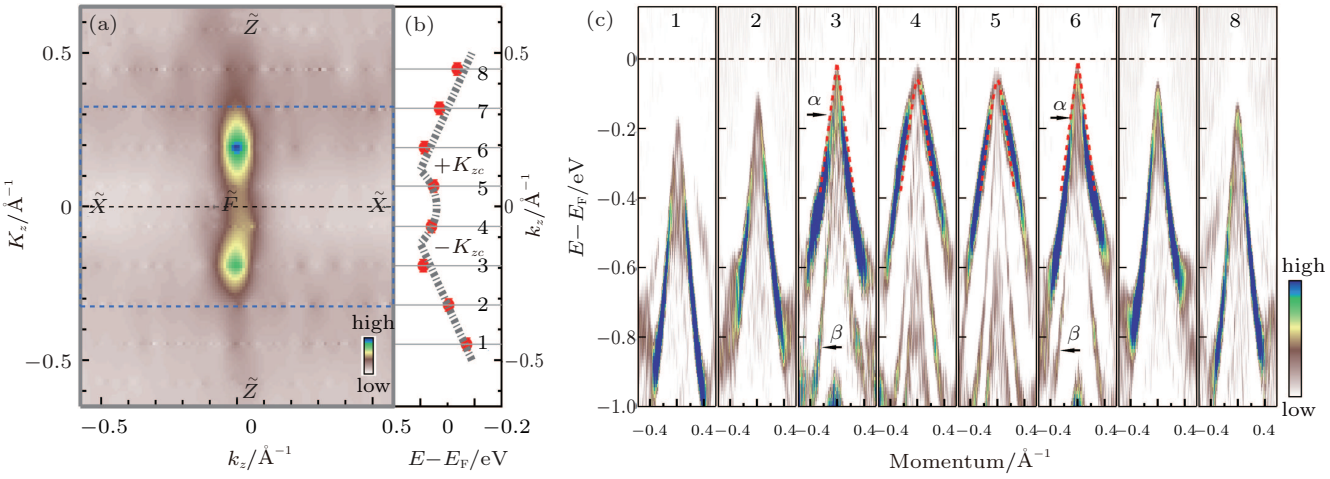


Fig. 9. Direct observation of a pair of three-dimensional Dirac cones on the (100) surface of Na_3Bi. (a) Fermi surface near the zone center measured on the (100) surface with a photon energy of 56 eV. The two spot-like features along the $\widetilde{Z}$–$\widetilde{\Gamma}$–$\widetilde{Z}$ direction, symmetrically located with respect to the zone center, are associated with the three-dimensional bulk Dirac nodes in Na_3Bi. (b) Energy position of the α band top (red cirlces) in panel (c) as a function of k_z. The gray dashed line is the guide to the eyes. (c) Band structures taken at different k_z along the $\widetilde{X}$–$\widetilde{\Gamma}$–$\widetilde{X}$ direction as sketched in panel (b). The band images are obtained by the second derivative of the original data with respect to the energy. The red dashed lines are fitted curves considering the Dirac cone shape.

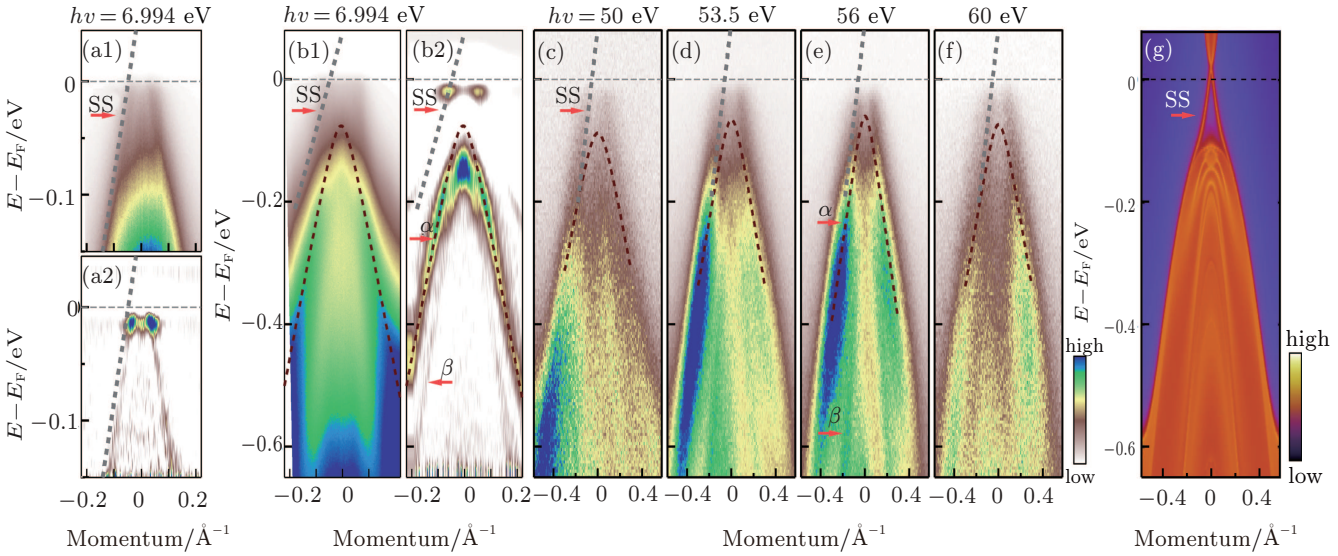


Fig. 10. Identification of the coexistence of the surface states with the three-dimensional bulk Dirac bands on the (100) surface of Na_3Bi. (a) Band structure along $\widetilde{X}$–$\widetilde{\Gamma}$–$\widetilde{X}$ direction taken by 6.994 eV VUV-laser ARPES. (a1) is the original data while (a2) is the second derivative image of (a1) with respect to energy. (b) Band structure along $\widetilde{X}$–$\widetilde{\Gamma}$–$\widetilde{X}$ direction over a large energy range taken by 6.994 eV VUV-laser ARPES. (b1) is the original data while (b2) is the second derivative image of (b1) with respect to energy. The bulk bands are marked by α and β in (b2). The gray dashed line is a guide to eyes for the SS band. (c)–(f) Band structures along $\widetilde{X}$–$\widetilde{\Gamma}$–$\widetilde{X}$ direction on the (100) surface taken by ARPES with different photon energies. (g) The theoretically calculated band structure along $\widetilde{X}$–$\widetilde{\Gamma}$–$\widetilde{X}$ direction on the (100) surface with surface states labeled as SS.

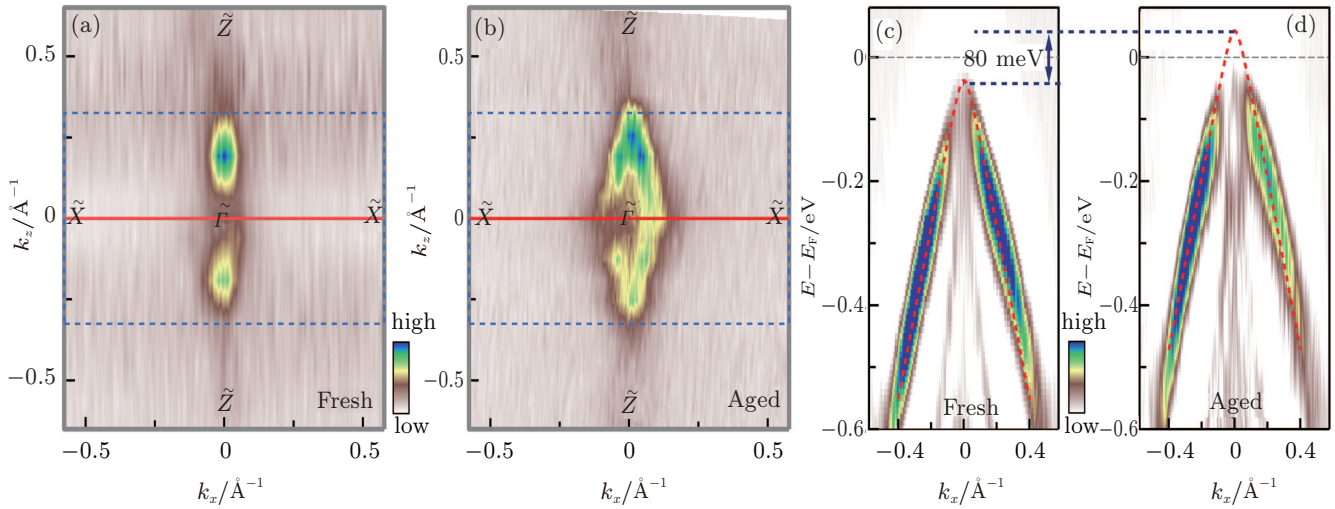


Fig. 11. Sample ageing effect on the Fermi surface and band structure of Na_3Bi. (a) Fermi surface measured by 56 eV photons on a fresh Na_3Bi (100) surface. (b) Fermi surface of the same (100) surface measured by 56 eV photons about 2 hours after cleaving. (c) Band structure measured on a fresh Na_3Bi (100) surface along the $\widetilde{X}$–$\widetilde{\Gamma}$–$\widetilde{X}$ cut indicated by a red line in panel (a). (d) Band structure measured on an aged Na_3Bi (100) surface along the $\widetilde{X}$–$\widetilde{\Gamma}$–$\widetilde{X}$ cut indicated by a red line in panel (b). An energy shift downward by ~80 meV is observed that indicates a hole doping effect during the sample aging process in vacuum.

the $\widetilde{\Gamma}$ point crosses the Fermi level (Fig. 11(d)). It turns out that there is a band shift upwards by about 80 meV during the sample aging of about two hours which causes hole doping into the sample. This indicates that the aging control of the sample during the ARPES measurements of Na_3Bi is crucial for the revelation of the bulk 3D dirac nodes and the nontrivial arc Fermi surface.

Having identified the 3D bulk Dirac nodes and the surface state, we take further investigations to resolve the unique Fermi surface arcs connecting the two 3D Dirac nodes on the (100) surface of the Na_3Bi. Figures 12(a)–12(f) show the constant energy contours at different binding energies measured on the (100) surface of Na_3Bi with a photon energy of 56 eV. The red and gray dashed lines are drawn for the bulk Dirac nodes and surface bands, respectively. For comparison, the calculated results are also presented in Figs. 12(g)–12(l). In Figs. 12(a)–12(f), the spectral weight that connects the two bulk Dirac nodes and takes a unique arc shape originates from the surface state, which can be more clearly observed when the binding energy is above 60 meV. The calculated results (Figs. 12(g)–12(l)) also show that the nontrivial surface state can penetrate deep below the Fermi level, forming rugby-like arc contours. The surface state we observe here matches well with the theoretical calculations.[25] The overall evolution of

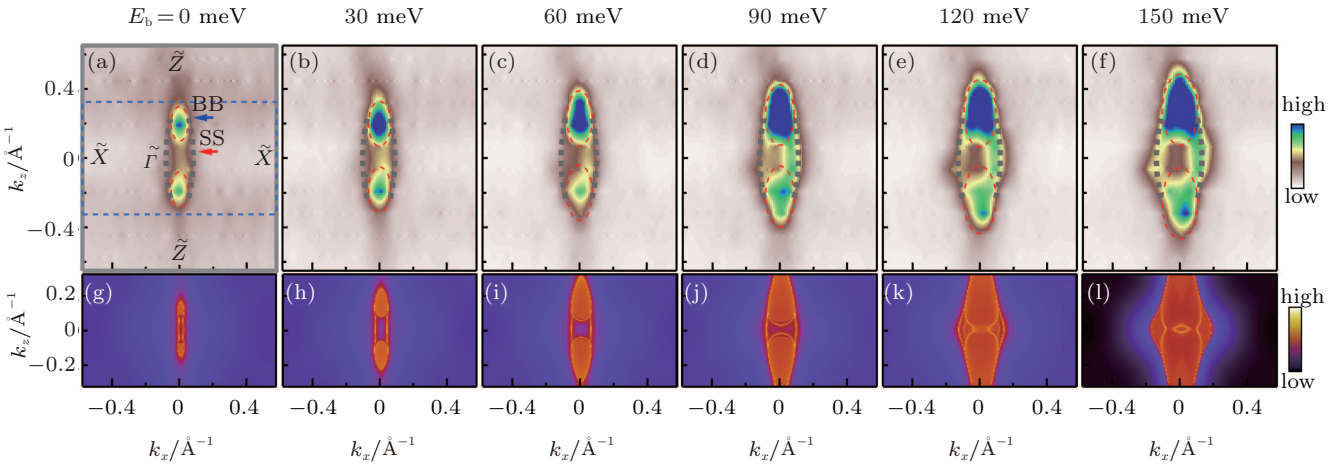


Fig. 12. The three-dimensional bulk Dirac nodes and the Fermi arc surface states that connect the nodes on the (100) surface of Na_3Bi. (a)–(f) The Fermi surface and constant energy contours at different binding energies measured using a photon enerngy of 56 eV on the (100) surface of Na_3Bi. The red and gray dashed lines are sketched for the bulk Dirac nodes and surface states, respectively. Labels of BB and SS stand for the bulk bands and surface bands, respectively. The first surface Brillouin zone, defined directly by the real space crystal structure in Fig. 1(a), is indicated by blue dashed lines. (g)–(l) The calculated results corresponding to the experimental data in panels (a)–(f), for comparison.

the two bulk Dirac nodes and the arc surface state with the binding energy are well reproduced from the theoretical calculations, except for the issue of the doubling length along k_z as mentioned above. Our ARPES results on the (100) surface are therefore consistent with the theoretical predictions of the 3D Dirac nodes and the Fermi arc structure on the Na_3Bi surface.

4. Conclusions

We have carried out comprehensive high-resolution angle-resolved photoemission (ARPES) measurements on the two cleaved surfaces, (001) and (100), of Na_3Bi. On the (001) surface, by comparison with theoretical calculations, we provide a proper assignment of the observed bands, and in particular, pinpoint the band that is responsible for the formation of the three-dimensional Dirac cones. We observe clear evidence of 3D Dirac cones in the three-dimensional momentum space by directly measuring on the k_x–k_y plane and by varying the photon energy to get access to different out-of-plane k_zs. In addition, we reveal new features around the Brillouin zone corners that may be related with surface reconstruction. On the (100) surface, our ARPES measurements over a large momentum space raise an issue on the selection of the basic Brillouin zone in the (100) plane. We directly observe two isolated 3D Dirac nodes on the (100) surface. We observe the signature of the Fermi-arc surface states connecting the two 3D Dirac nodes that extend to a binding energy of ∼150 meV before merging into the bulk band. Our observations constitute strong evidence on the existence of the Dirac semimetal state in Na_3Bi that are consistent with previous theoretical and experimental work. In addition, our results provide new information to clarify on the nature of the band that forms the 3D Dirac cones, on the possible formation of surface reconstruction of the (001) surface, and on the issue of basic Brillouin zone selection for the (100) surface. These observations are important in further study of the topological nature and transport properties of the three-dimensional Dirac semimetal Na_3Bi.

References

[1] Wan X, Turner A M, Vishwanath A and Savrasov S Y 2011 *Phys. Rev. B* **83** 205101
[2] Turner A M and Vishwanath 2013 arXiv:1301.0330
[3] Yang B J and Nagaosa N 2014 *Nat. Commun.* **5** 4898
[4] Weng H, Dai X and Fang Z 2014 *MRS Bulletin* **39** 849
[5] Nielsen H B and Ninomiya M 1981 *Nucl. Phys. B* **185** 20
[6] Nielsen H B and Ninomiya M 1981 *Nucl. Phys. B* **193** 173
[7] Murakami S 2007 *New J. Phys.* **9** 356
[8] Murakami S 2011 *Physica E* **43** 748
[9] Balents L 2011 *Physics* **4** 36
[10] Xu G, Weng H, Wang Z, Dai X, and Fang Z 2011 *Phys. Rev. Lett.* **107** 186806
[11] Burkov A A and Balents L 2011 *Phys. Rev. Lett.* **107** 127205
[12] Burkov A A, Hook M D and Balents L 2011 *Phys. Rev. B* **84** 235126
[13] Zyuzin A A, Wu S and Burkov A A 2012 *Phys. Rev. B* **85** 165110
[14] Halasz G B and Balents L 2012 *Phys. Rev. B* **85** 035103
[15] Young S M, Zaheer S, Teo J C Y, Mele E J and Rappe A M 2012 *Phys. Rev. Lett.* **108** 140405
[16] Wang Z, Sun Y, Chen X, Franchini C, Xu G, Weng H, Dai X and Fang Z 2012 *Phys. Rev. B* **85** 195320
[17] Liu Z, Zhou B, Zhang Y, Wang Z, Weng H, Prabhakaran D, Mo S K, Shen Z, Fang Z, Dai X, Hussain Z and Chen Y 2014 *Science* **343** 864
[18] Zhang Y, Liu Z, Zhou B, Kim Y, Hussain Z, Shen Z, Chen Y and Mo S K 2014 *Appl. Phys. Lett.* **105** 031901
[19] Wen J, Guo H, Yan C, Wang Z, Chang K, Deng P, Zhang T, Zhang Z, Ji S, Wang L, He K, Ma X, Chen X and Xue Q 2014 *Chin. Phys. Lett.* **31** 116802
[20] Wen J, Guo H, Yan C, Wang Z, Chang K, Deng P, Zhang T, Zhang Z, Ji S, Wang L, He K, Ma X, Chen X and Xue Q 2015 *Applied Surface Science* **327** 213
[21] Xu S, Liu C, Kushwaha S K, Sankar R, Krizan J W, Belopplski I, Neupane M, Bian G, Alidoust N, Chang T R, Jeng H J, Huang C, Tsai W, Lin H, Shibayev P P, Chou F, Cava R J and Hasan M Z 2015 *Science* **347** 294
[22] Xu S, Liu C, Belopolski I, Kushwaha S K, Sankar R, Krizan J W, Chang T R, Polley C M, Adell J, Balasubramanian T, Miyamoto K, Alidoust N, Bian G, Neupane M, Jeng H J, Huang C , Tsai W, Okuda T, Bansil A, Chou F, Cava R J, Lin H and Hasan M Z 2015 *Phys. Rev. B* **92** 075115

[23] Xiong J, Kushwaha S K, Liang T, Krizan J W, Hirschberger M, Wang W, Cava R J and Ong N P 2015 *Science* **350** 6259

[24] Kushwaha S K, Krizan J W, Feldman B E, Gyenls A, Randerla M, Xiong J, Xu S-Y, Aldoust N, Belopolski I, Liang T, Hasan M Z, Ong N P, Yazdani A and Cava R J 2015 *APL Mater.* **3** 041504

[25] Gorbar E V, Miransky V A, Shovkovy I A and Sukhachov P O 2015 *Phys. Rev. B* **91** 235138

[26] Wang Z, Weng H, Wu Q, Dai X and Fang Z 2013 *Phys. Rev. B* **88** 125427

[27] Liu Z, Jiang J, Zhou B, Wang Z, Zhang Y, Weng H, Prabhakaran D, Mo S K, Peng H, Dudin P, Kim T, Hoesch M, Fang Z, Dai X, Shen Z, Feng D, Hussain Z and Chen Y 2014 *Nat. Mater.* **13** 677

[28] Neupane M, Xu S, Sankar R, Alidoust N, Bian G, Liu C, Belopolski I, Chang T R, Jeng H T, Lin H, Bansil A, Chou F and Hasan M Z 2014 *Nat. Commun.* **5** 3786

[29] Borisenko S, Gibson Q, Evtushinsky D, Zabolotnyy Vand Cava R J 2014 *Phys. Rev. Lett.* **113** 027603

[30] Yi H, Wang Z, Chen C, Shi Y, Feng Y, Liang A, Xie Z, He S, He J, Peng Y, Liu X, Liu Y, Zhao L, Liu G, Dong X, Zhang J, Nakatake M, Arita M, Shimada K, Namatame H, Taniguchi M, Xu Z, Chen C, Dai X, Fang Z and Zhou X 2014 *Scientific Reports* **4** 6106

[31] Jeon S, Zhou B B, Gyenis A, Feldman B E, Kimchi I, Potter A C, Gibson Q D, Cava R J, Vishwanath A and Yazdani A 2014 *Nat. Mater.* **13** 851

[32] He L, Hong X, Dong J, Pan J, Zhang Z, Zhang J and Li S 2014 *Phys. Rev. Lett.* **113** 246402

[33] Novoselov K S, Geim A K, Morozov S V, Jiang D, Katsnelson M I, Grigorieva I V, Dubonos S V and Firsov A A 2005 *Nature* **438** 197

[34] Zhang Y, Tan Y W, Stormer H L and Kim P 2005 *Nature* **438** 201

[35] Hasan M Z and Kane C L 2010 *Rev. Mod. Phys.* **82** 3045

[36] Qi X and Zhang S 2011 *Rev. Mod. Phys.* **83** 1057

[37] Weyl H 1929 *Z. Phys.* **56** 330

[38] Weng H, Fang C, Fang Z, Bernevig B A and Dai X 2015 *Phys. Rev. X* **5** 011029

[39] Huang S, Xu S, Belopolski I, Lee C C, Chang G, Wang B, Alidoust N, Bian G, Neupane M, Zhang C, Jia S, Bansil A, Lin H and Hasan M Z 2015 *Nat. Commun.* **6** 7373

[40] Lv B, Weng H, Fu B, Wang X, Ma J, Richard P, Huang X, Zhao L, Chen G, Fang Z, Dai X, Qian T, Shi M and Ding H 2015 *Phys. Rev. X* **5** 031013

[41] Lv B, Xu N, Weng H, Ma J, Richard P, Huang X, Zhao L, Chen G, Matt C E, Bisti F, Strocov V N, Mesot J, Fang Z, Dai X, Qian T, Shi M and Ding H 2015 *Nat. Phys.* **11** 724

[42] Xu S, Alidoust N, Neupane M, Bian G, Zhang C, Sankar R, Chang G, Yuan Z, Lee C C, Huang S, Zheng H, Ma J, Sanchez D S, Wang B, Bansil A, Chou F, Shibayev P P, Lin H, Jua S and Hasan M Z 2015 *Science* **349** 613

[43] Yang L, Liu Z, Sun Y, Peng H, Yang H F, Zhang T, Zhou B, Zhang Y, Guo Y F, Rahn M, Prabhakaran D, Hussain Z, Mo S K, Felser C, Yan B and Chen Y 2015 *Nat. Phys.* **11** 9

[44] Xu D, Du Y, Wang, Z, Li Y, Niu X, Yao Q, Pavel D, Xu Z, Wan X and Feng D 2015 *Chin. Phys. Lett.* **32** 107101

[45] Lu L, Wang Z, Ye D, Ran L, Fu L, Joannopoulos J D and Soljacic M 2015 *Science* **349** 622

[46] Liu G, Wang G, Zhu Y, Zhang H, Zhang G, Wang X, Zhou Y, Zhang W, Liu H, Zhao L, Meng J, Dong X, Chen C, Xu Z and Zhou X 2008 *Rev. Sci. Instru.* **79** 023105

[47] Perdew J P, Burke K and Ernzerhof M 1996 *Phys. Rev. Lett.* **77** 3865

[48] Blaha P, Schwarz K, Madsen G, Kvasnicka D and Luitz J *WIEN2K Package*

[49] Hufner J 1985 *Photoelectron Spectroscopy: Principles and Applications* (Berlin: Springer-Verlag) pp. 353–357